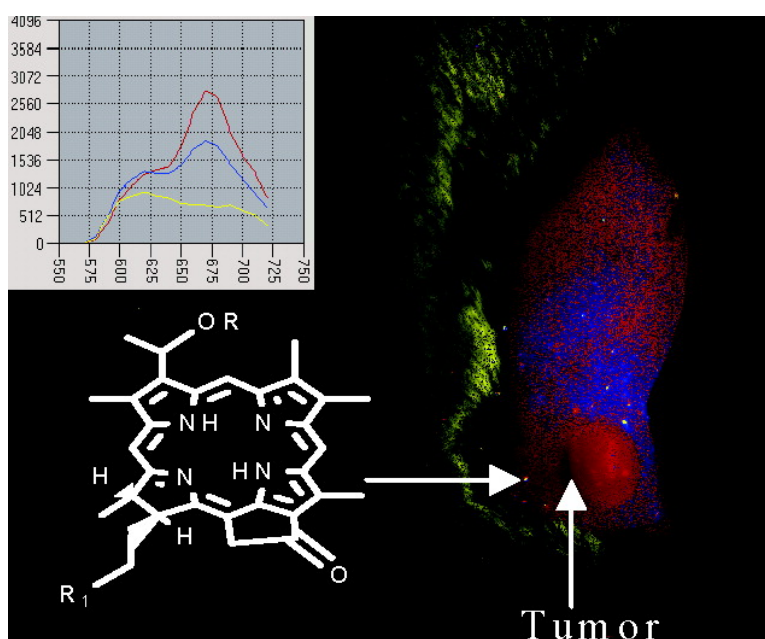Article

# Multimodality Agents for Tumor Imaging (PET, Fluorescence) and Photodynamic Therapy. A Possible "See and Treat" Approach

Suresh K. Pandey, Amy L. Gryshuk, Munawwar Sajjad, Xiang Zheng, Yihui Chen, Mohei M. Abouzeid, Janet Morgan, Ivan Charamisinau, Hani A. Nabi, Allan Oseroff, and Ravindra K. Pandey

Tumor

## More About This Article

Additional resources and features associated with this article are available within the HTML version:

- Supporting Information
- Links to the 9 articles that cite this article, as of the time of this article download
- Access to high resolution figures
- Links to articles and content related to this article
- Copyright permission to reproduce figures and/or text from this article

View the Full Text HTML

# Multimodality Agents for Tumor Imaging (PET, Fluorescence) and Photodynamic Therapy. A Possible "See and Treat" Approach

Suresh K. Pandey,[†] Amy L. Gryshuk,[†,‡] Munawwar Sajjad,[*,§] Xiang Zheng,[†] Yihui Chen,[†] Mohei M. Abouzeid,[§] Janet Morgan,[‡] Ivan Charamisinau,[‡] Hani A. Nabi,[§] Allan Oseroff,[‡] and Ravindra K. Pandey[*,†]

*PDT Center and Department of Dermatology, Roswell Park Cancer Institute, Buffalo, New York 14263, and Department of Nuclear Medicine, State University of New York, Buffalo, New York 14214*

*Received May 5, 2005*

Methyl 3-(1′-*m*-iodobenzyloxyethyl)-3-devinylpyropheophorbide-*a* (**2**), obtained in a sequence of reactions from pyropheophorbide-*a* (a chlorophyll-*a* derivative), was found to be a promising imaging agent and a photosensitizer for photodynamic therapy (PDT). The electrophillic aromatic iodination of the corresponding trimethylstannyl intermediate with Na[124]I in the presence of an Iodogen bead afforded [124]I-labeled photosensitizer **4** with >95% radioactive specificity. In addition to drug-uptake, the light fluence and fluence rate that were used for the light treatment had a significant impact in long-term tumor cure. The iodo photosensitizer **2** (nonlabeled analogue of **4**) produced 100% tumor cure (5/5 mice were tumor free on day 60) at a dose of 1.5 $\mu$mol/kg and a light dose of 128 J/cm$^2$, 14 mW/cm$^2$ for 2.5 h ($\lambda_{max}$ 665 nm) at 24 h postinjection. The photosensitizer also showed promising tumor fluorescence and PET imaging ability. Our present work demonstrates the utility of the first [124]I-labeled photosensitizer as a "multimodality agent", which could further be improved by using more tumor-avid and/or target-specific photosensitizers.

## Introduction

Histological sections are the gold standard for phenotypic analysis of cancer cells but require biopsy or autopsy, which precludes further biologic analysis. With the advancement in "noninvasive" imaging technologies and imaging probes, the field of imaging science is growing exponentially, and therefore, fusion of in vivo imaging techniques (CT, SPECT, PET, bioluminescence, fluorescence, MRI) to observe events at the molecular and cellular level are expected to accelerate the drug discovery and development process.[1,2] The imaging of specific molecular targets that are associated with cancer should allow earlier diagnosis and better assessment to oncology patients.

With the latest advent of small-animal micro-PET systems, the resolution of which could reach near 1.2 mm, PET has widened its appeal for research at the drug development stage, as it allows studying the drug distribution in vivo. By using radiolabeled tracers, which are injected in nontherapeutic doses, 3-D images can be reconstructed by a computer to show the location(s) and concentration of the tracer, which then can be coupled with a therapeutic agent to treat the target. The approaches now focus on the development of a common molecule that is first used in low mass (as a radioactive material) to image and measure the target function, and then the mass of the molecule is increased by using the same unlabeled compound at therapeutic levels to treat the target function.[3] Drugs labeled with [11]C ($t_{1/2}$ = 20.4 min) and [18]F ($t_{1/2}$ = 110 min) are the most common used

PET isotopes. The short half-life of ^{11}C and ^{18}F limits their use in studies involving monoclonal antibodies and other molecules such as photosensitizers (PS), which take long time (hours instead of minutes) for accumulation in a tumor.

[124]I is a more suitable candidate, as it has a half-life of 4.2 days and is compatible for the sequential imaging using microPET due to its longer biological half-life. Labeling techniques with radioiodine (^{123}I, [124]I, etc.) are well-defined and one can obtain the labeled products in good yield with radiochemical purity.[4−6] Despite the complex decay scheme of [124]I, which results in only 25% abundance of positron (compared with 100% positron emission of ^{18}F), in vivo quantitative imaging with [124]I-labeled antibodies has been successfully carried out under realistic conditions using PET/CT scanner,[7−10] and 3D-dosimetry has been performed.[11] As for now, [124]I has been used to label a variety of biomolecules, viz. monoclonal antibodies, minibodies and dibodies,[4,12,13] annexinV,[14] iodoazomycingalactoside (IAZG),[15] and 5-iodo-2′-fluoro-1-$\beta$-D-arabinofuranosyluracil (FIAU).[16−20] There are a few reports in the PDT field in which various ^{18}F-based radiotracers, FDG,[21] ^{18}F-FHBG {9-(4-^{18}F-fluoro-3-hydroxymethyl-butyl)guanine},[22] and FLT (3′-deoxy-3′-18F-fluorothymidine),[23] or ^{125}I-labeled photosensitizer[24] have been used to monitor cellular events post-PDT in mice at certain intervals of time.

For quite some time we have been interested in using certain tumor-avid porphyrin-based molecules as vehicles to transfer the desired nuclide to the target-site for nuclear imaging. The advantages are that these compounds are "bifunctional"; i.e., they are both selective imaging agents as well as efficacious PS for PDT. In our initial study, we conjugated 3-(1′-*m*-hexyloxyethyl)-3-devinylpyropheophorbide-*a* (HPPH), a tumor-avid and effective PS (currently in phase II human

* Corresponding authors. M.S.: phone, 716-838-5889, ext. 118; fax, 716-838-4918; e-mail, msajjad@buffalo.edu. R.K.P.: phone: 716-845-3203; fax: 716-845-8920; e-mail: ravindra.pandey@roswellpark.org.
† PDT Center, Roswell Park Cancer Institute.
‡ Department of Dermatology, Roswell Park Cancer Institute.
§ State University of New York.

clinical trials) with mono- and dibisaminoethanethiols ($N_2S_2$ ligand).[25] The in vivo biodistribution data of the related ^{99m}Tc complexes were collected in rats bearing Ward colon tumors at 4 and 24 h postinjection. These large tumors had high concentrations of the tracer; however, the short 6-h half-life time of ^{99m}Tc was found to be incompatible with the 24 h imaging time (HPPH takes around 24 h to reach maximum accumulation in tumors), suggesting that the introduction of a longer lived isotope (e.g., ^{111}In) in tumor-avid PS could provide a more useful scanning agent with phototherapeutic properties. We have recently prepared certain indium-(III) complexes of HPPH, and they were found to be tumor-avid. In preliminary screening, compared to HPPH, the corresponding In(III) analogue [In(III) HPPH] was found to be 40-fold more effective in vitro and 8-fold more effective in vivo with limited skin phototoxicity (no skin phototoxicity was observed at day 3 postinjection of the PS).[26] The synthesis and biological studies of the corresponding ^{111}In analogue are currently in progress at our laboratory.

Besides nuclear imaging, planar optical imaging (i.e., 2D fluorescence images of the tissue investigated by using appropriate filters) has also received much attention because of its ease of implementation, operational simplicity, low cost, and recent development of novel fluorescent probes.[27] In general, the magnitude of any fluorescent signal depends on the local fluorophore concentration and is attenuated by chromophore−chromophore and chromophore−local environment interactions. Hence, delivering an appropriately large payload of emitters to a specific site is a challenge that must be addressed when designing new photonic beacons for in vivo imaging.[28] Development of near-infrared (NIR) molecular probes with high specificity, selectivity, sensitivity, and stability is highly desirable for imaging diseases in small animals. One approach to achieve selectivity in oncology is the ability to take advantage of the overexpression of specific receptors and proteins on certain tumor cells as a means to explore various targets in tumors. However, conjugation of a dye to antibodies and other large targeting molecules (such as synthetic dendrimers, nanoparticles, quantum dots, and other polyvalent compounds) is not easy to control and ends up in lower yields with an unknown ratio of dye attached. The resulting molecular constructs may quench fluorescence, induce aggregation, disrupt bioactive conformations of adjacent small molecules, and destabilize the chromophore systems because of their exposure to harsh and metabolically active mediums, besides being hampered by many factors, including low diffusion rates into tumors, rapid uptake by liver, and the potential to elicit adverse immunogenic reactions.[29] Recent studies have focused on developing dye (viz., fluorescein, carbocyanine) conjugates of small bioactive molecules (like glucose, peptides) to improve rapid diffusion to target tissue and to identify and optimize new molecular beacons.[30] Furthermore, optical imaging is an emerging diagnostic method, and its acceptance in clinical practice requires validation of images obtained with established nuclear imaging modalities, such as PET.

In recent years, the pyropheophorbide analogues have created a great interest in fluorescence imaging and PDT. For example, the hexyl ether derivative of py-

ropheophorbide-*a* (HPPH or Photochlor) is currently in phase II human clinical trials at our institute.[31] The related 2-deoxyglucose derivative, named Pyro-2DG, has been reported as a glucose transport targeted photosensitizer for detection and treatment of cancer.[32] The HPPH−carotene conjugate has also been reported as an NIR imaging agent.[33] In this novel structure, the carotene moiety quenches the singlet oxygen produced by the light exposure and thereby completely eliminates its photosensitizing ability and skin phototoxicity.

In our present study, as a "proof of principle" approach, our main objective was to investigate the utility of [124]I-labeled PS in imaging and therapy. Therefore, in our initial study the readily available pyropheophorbide-*a* was modified to create a "Trifunctional Agent" for dual imaging (PET and fluorescence) and PDT. Our preliminary data demonstrate the feasibility of developing a single agent for tumor imaging (PET, fluorescence) and therapy (PDT). This approach provides an opportunity to expand our methodology in the future to a more tumor-avid long-wavelength-absorbing PS derived from other chlorins, phthalocyanines, and bacteriochlorin systems.

## Results and Discussion

**Chemistry.** Methyl 3-(1′-*m*-iodobenzyloxyethyl)pyropheophorbide-*a* (**2**) was synthesized by following the methodology developed in our laboratory for the preparation of the related alkyl ether analogues.[34] In brief, methyl pyropheophorbide-*a* (**1**) was reacted with 33% HBr/acetic acid. The intermediate bromo derivative obtained after removing the acids was reacted with 3-iodobenzyl alcohol in the presence of anhydrous potassium carbonate to yield the pyropheophorbide analogue **2**, which was used for therapy (PDT) and fluorescence imaging. To investigate the utility of the same molecule for PET imaging, the iodo derivative **2** was first converted into trimethyltin analogue **3** by reacting with hexamethyleneditin and a catalytic quantity of bistriphenylphosphinepalladium(II) dichloride. Compound **3** upon reacting with Na[124]I in the presence of Iodogen bead[5] yielded [124]I-labeled compound **4** (Scheme 1) and was purified by preparative HPLC (Figure 1).

**In Vitro Uptake, Localization, and Phototoxicity. Pyroiodobenzyl Ether 2 Showed Higher Tumor Uptake than HPPH.** The in vitro uptake of HPPH was compared with PS **2** in RIF cells at 37 °C. As can be seen from Figure 2, at 3 h incubation, both photosensitizers produced similar uptake. However, PS **2** showed a significant increase in uptake with time and at the 24-h incubation it was 2.5-fold higher than that observed for HPPH, which remained constant.

**The Subcellular Localization of Iodobenzyl Ether Analogue Was Different Than HPPH with Limited PBR Binding Affinity.** Peripheral benzodiazepine receptor (PBR) is an 18-kDa protein of the outer mitochondrial membrane,[35] which is involved in numerous functions including steroid biosynthesis, mitochondrial respiration, heme biosynthesis, cell proliferation, and calcium channel modulation.[35] Elevated PBR expression is also related to certain cancers, such as those of breast, colon−rectum, and prostate tissue and has been proposed as a novel prognostic indicator of an aggressive phenotype for these indications.[36] Another

**Scheme 1.** Preparation of HPPH and the Related [124]I-Labeled Photosensitizer from Methyl Pyropheophorbide-*a*
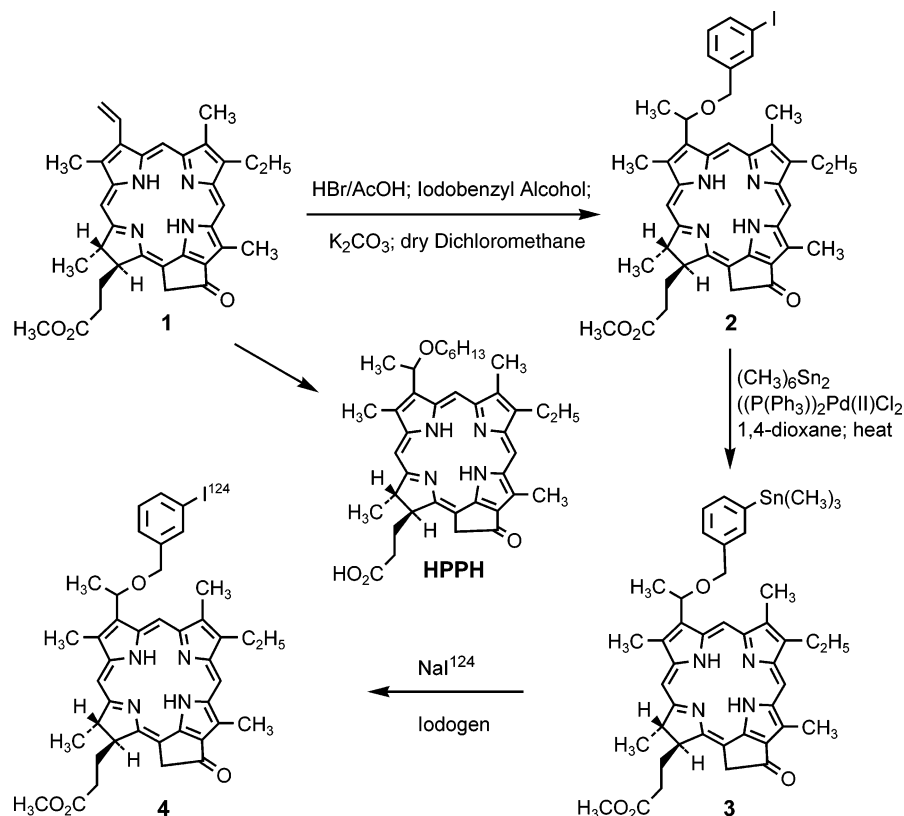


intriguing aspect of the PBR is its association with photodynamic therapy (PDT). A previous report from our laboratory has shown the importance of the PBR as a binding site for a series of chlorin-type PS such as pyropheophorbide-*a* ethers.[37] It was found that the PDT
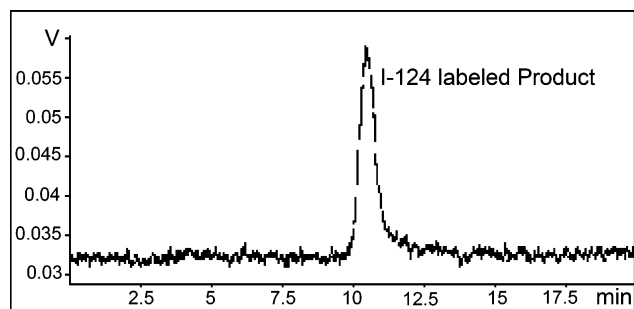


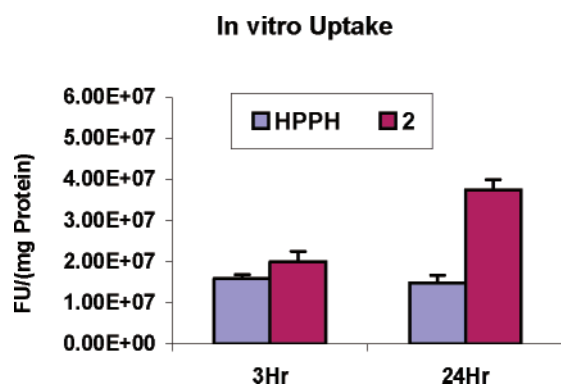**Figure 1.** HPLC Chromatogram of [124]I-labeled photosensitizer **4**.



**Figure 2.** Comparative in vitro uptake of **2** and HPPH at an equimolar concentration (0.25 $\mu$M) in RIF cells at 3 and 24 h postincubation.

effect was inhibited by PK11195 [1-(2-chlorophenyl)-*N*-methyl-*N*-(1-methylpropyl)-isoquinoline-3-carboxamide] for the active derivatives of the alkyl ether derivatives of pyropheophorbide-*a*, and a limited affect was found for the less active analogues. However, no direct correlation between PBR displacement ability and PDT efficacy was observed.

The in vitro intracellular localization of **2** in RIF cells was found to depend on the time interval. For example, the mitochondrial colocalization of **2** with Mitotracker Green (MTG) was observed within the first 2 h of cellular uptake (Figure 4C), where it was found to have a slight displacement with ^{3}H-PK11195 (a standard peripheral benzodiazepine receptor binder) (Figure 3). Over time, **2** shifted rapidly to the Golgi apparatus, as seen by colocalization of **2** with the red fluorescence emitted by Bodipy FL aggregates that accumulate in
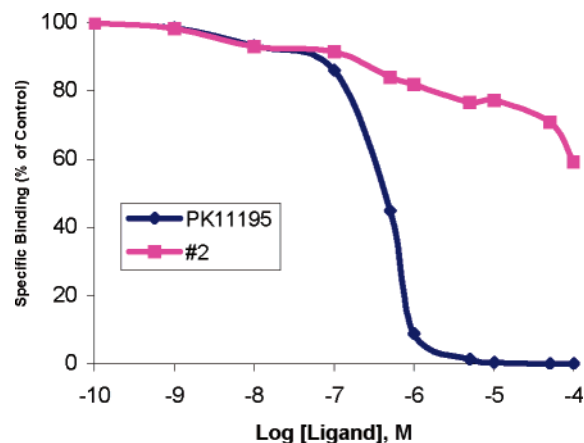


**Figure 3.** Comparative in vitro displacement of compound **2** and PK11195 (known PBR probe) with 3HPK11195.
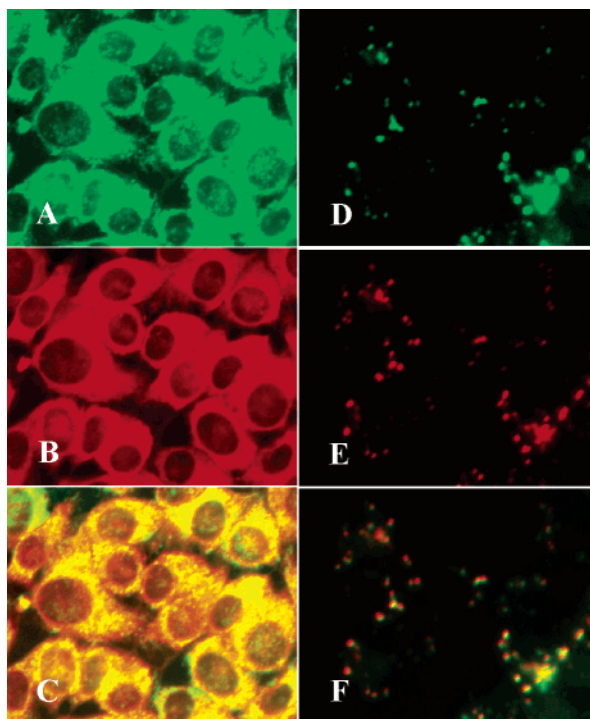
**Figure 4.** Comparative subcellular localization of Mitotracker Green (MTG): (A) **2**, (B) MTG (for mitochondria), (C) overlay of parts A and B, (D) Bodipy C5 ceramide (for golgi apparatus), (E) **2**, and (F) overlay of parts D and E in RIF cells.
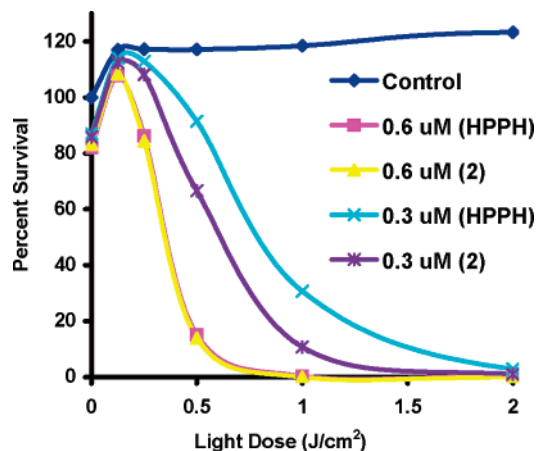


**Figure 5.** Comparative in vitro photosensitizing activity of **2** and HPPH at variable drug concentrations and light doses in RIF tumor cells at 24 h postincubation.

the Golgi complex (Figure 4F). No colocalization of compound **2** was observed with Fluospheres, which rules out its presence in lysosomes (not shown). HPPH under similar experimental procedures was found to localize in mitochondria and was independent of incubation time.

**Both Iodobenzyl Ether Analogue 2 and HPPH Were Equally Effective in Vitro.** The in vitro phototosensitizing ability of HPPH and the iodobenzyl ether derivative **2** was compared under variable experimental conditions (MTT assay, see Experimental Section) in RIF cells. As can be seen from Figure 5, at higher drug concentration (0.6 $\mu$M), both PS **2** and HPPH produced similar efficacy. However, at a lower drug concentration (0.3 $\mu$M), PS **2** was found to be slightly more effective at 24 h postincubation.
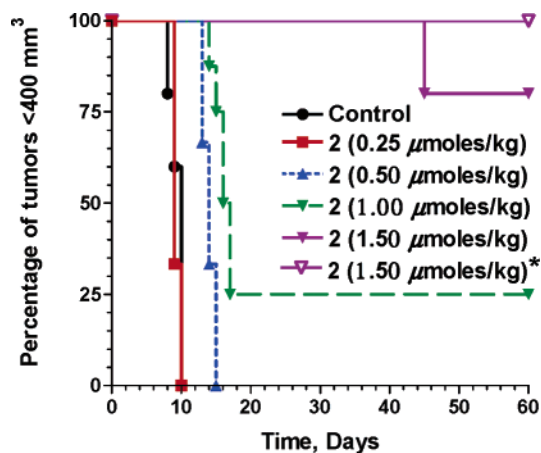


**Figure 6.** In vivo photosensitizing efficacy of PS **2** at variable concentrations. C3H mice (five mice/group) bearing RIF tumors were exposed to a laser light (665 nm, 135 J/cm$^2$, 75 mW/cm$^2$) for 30 min at 24 h postinjection (*665 nm, 128 J/cm$^2$, 14 mW/cm$^2$ for 2°32′23″ at 24 h postinjection). Mice that did not show any tumor regrowth were considered cured (tumor was flat).

**In Vivo Phototoxicity. Photosensitizer 2 Was Found To Be Effective in Vivo.** For evaluating the in vivo PDT efficacy of PS **2**, the C3H mice (five mice/group) bearing RIF tumors (4−5 mm in diameter) were injected intravenously at variable drug doses (0.25, 0.5, 1.0, and 1.5 $\mu$mol/kg). The tumored area was then irradiated with a 1 cm$^2$ laser light (665 nm, 135 J/cm$^2$, 75 mW/cm$^2$ for 30 min) at 24 h postinjection. The tumor regrowth was observed daily, and when the tumor size reached the threshold of 400 mm$^3$, the mice were sacrificed. From the results summarized in Figure 6, it can be seen that at lower concentrations (0.25 and 0.50 $\mu$mol/kg) PS **2** was not very effective. However, at higher doses, a significant long-term tumor response (tumor-cure) was observed. At a dose of 1.5 $\mu$mol/kg, the PS was found to be quite effective (at day 60, 8/10 mice were tumor free, $P = 0.03$). The treatment parameters were optimized and at a variable light dose (665 nm, 128 J/cm$^2$, 14 mW/cm$^2$ for 150 min) we found that the tumor response was enhanced (5/5 mice were tumor free at day 60, $P = 0.034$). Such effect of light fluence and fluence rate has also been reported by other investigators[38,39] and is currently being practiced all over the world in human clinical trials for several indications.

**In Vivo Imaging: Pyropheophorbide Analogue 2 Produced High Tumor Uptake, As Determined by in Vivo Fluorescence Imaging.** PS **2** in organic solvents (CH$_2$Cl$_2$, THF) exhibits strong absorption at $\lambda_{max}$ 662 nm ($\epsilon = 47\,500$) and emission at 667 nm (strong) and 710 nm (weak), respectively. Its singlet oxygen production capability ($\phi$) is about 67%. On the basis of a small difference in the Stokes shift between the absorption and emission, compounds containing pyropheophorbide-$a$ system are not the "ideal" candidates for optical imaging. However, during our initial studies, our main objective was to establish a "proof of principle" concept by demonstrating the utility of tumor-avid PS in optical imaging. Therefore, due to a small shift (5 nm) between long-wavelength absorption and fluorescence, we exposed the tumor to laser light at 532 nm (weak absorption of the photosensitizer), and a strong fluorescence was recorded at 667 nm. These
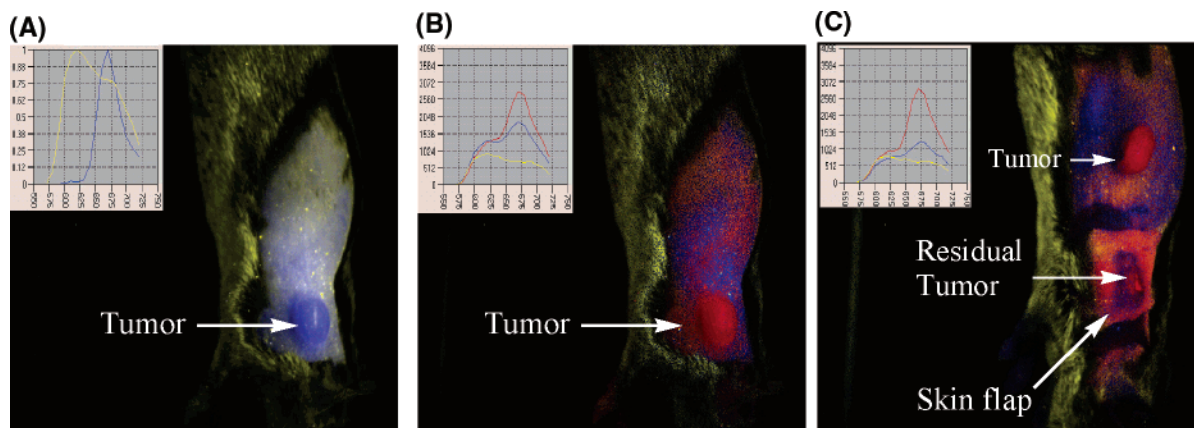
**Figure 7.** (A) Whole-body fluorescence reflectance images (FRI) of mice injected with photosensitizer (PS) **2** (1.5 $\mu$M/kg) at 24 h postinjection. The blue color represents fluorescence spectrum of PS **2**, while the yellow color represents the autofluorescence from the mouse (background). (B) Using the spectral unmixing program Nuance, the localization of PS **2** can be easily resolved between tumor (red spectra) and skin (blue spectra). The yellow color represents the hair of the mouse. (C) Fluorescence reflectance image (FRI) of the same mouse in which tumor is dissected out and kept on shaved skin far away from the original site. There is some drug in the skin flap (may contain residual tumor). Using the spectral unmixing program Nuance, the localization of PS **2** can be easily resolved between tumor, skin flap (red spectra), skin (blue spectra), and hair (yellow spectra) of the mouse.
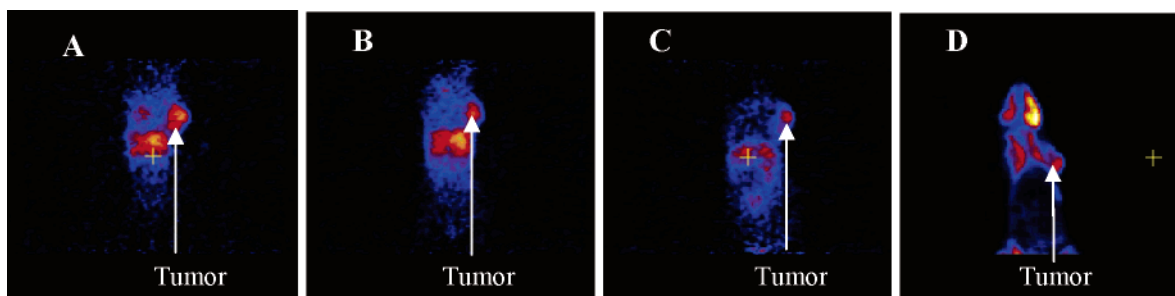


**Figure 8.** Comparative (PET) images of mice bearing RIF tumors injected with $^{124}$I-analogue **4** (50 $\mu$Ci) at 24 h (A), 48 h (B), and 72 h (C) postinjection of the drug, and with F-18 FDG (D) at 90 min postinjection. (As expected from the porphyrin-based compounds, the presence of **4** was evident in some other organs, especially in liver, spleen, and intestine). However, compared to 24 h, better contrast was observed at 48 and 72 h postinjection.

parameters could be used for imaging either superficial tumors or those that are not deeply seated.

In a typical in vivo experiment, nine (9) female C3H mice were subcutaneously injected with RIF tumor cells on the shaved right shoulder (posterior axilla region) and were imaged (a day before PDT treatment size of tumors which is 4 × 4 mm$^3$) to serve as self-background control. The mice were then injected with PS **2** at a therapeutic dose of 1.5 $\mu$mol/kg via tail vein and kept in the dark to rule out the possibility of any kind of photobleaching during the course of the experiment. Three (3) mice per group at 24-, 48-, and 72-h time intervals were imaged under anesthesia (ketamine/xylazine), and spectral unmixing showed that PS **2** localized mainly in the tumor area (Figure 7A,B). To visualize the actual localization of **2** in tumor versus the skin over the tumor, the tumor was surgically removed from its original site and placed away from its original site. Upon imaging the prominent fluorescence intensity of **2** was found in the tumor compared to the normal skin (skin away from tumor). A moderate level of fluorescence was also observed in the skin flap (minus the tumor), which contains tumor-feeding vasculature compared to normal skin (Figure 7C). Due to the limited penetration of visible light (532 nm), images from interior organs could not be obtained. Therefore, for imaging deeply seated tumors and other organs, it is necessary to have fluorochromes that exhibit abosorp-

tion near 800 nm, where tissue penetration is deeper. However, it is possible to perform a fluorescence-based biodistribution study in isolated organs and compared it to the $^{124}$I-based biodistribution study (Figure 9). The synthesis and biological evaluation of more tumor-specific long-wavelength-absorbing PS (700−800 nm) are currently in progress.

**The $^{124}$I-Labeled Photosensitizer 2 (Photosensitizer 4) Showed High Uptake in Tumor by PET Imaging.** For micro-PET studies, four female C3H mice/group were injected with RIF tumor cells on the shaved right shoulder (axilla region), and after 4 days, when the tumor size reached 3 × 3 mm$^3$ in dimension, the tumor was imaged prior to injection to serve as a self-control. Then FDG (150−200 $\mu$Ci) was injected in each mouse via tail vein and they were imaged for 20 min at 45 min postinjection. As can be seen from Figure 8D, F-18 FDG (a clinical PET imaging agent) rapidly circulates to all the metabolic sites, and it was difficult to distinguish between the tumor and the arm muscle. It clears rapidly from the system and did not provide any significant specificity for tumor alone. However, compared to F-18 FDG, when the $^{124}$I-labeled PS **4** (36−100 $\mu$Ci) was injected (via tail vein), a significant localization of PS **4** in tumor at 24, 48, 72 h postinjection was observed (Figure 8). If necessary, the thyroid image due to free iodine ($^{124}$I) can be blocked by injecting cold
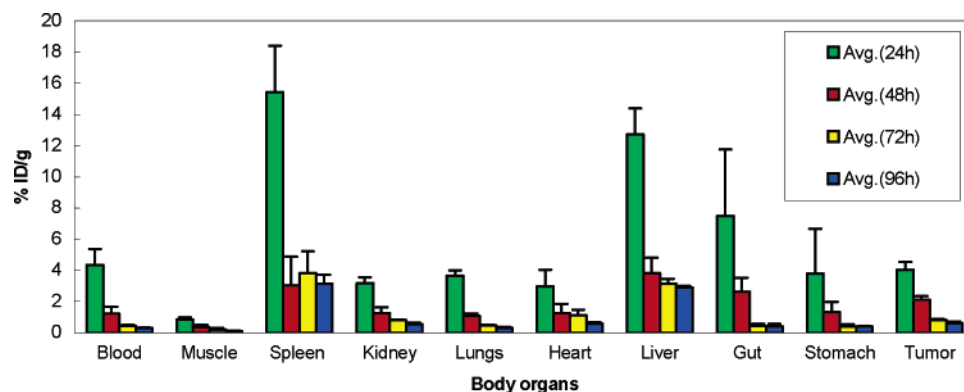
**Figure 9.** Biodistribution results of $^{124}$I-labeled PS **4** (%ID/g) in some selected organs of mice (three mice/group) at 24, 48, 72, and 96 h postinjection.

**Table 1.** Biodistribution Results of $^{124}$I-Labeled PS 4 in Some Selected Organ of Mice (three mice/group) at 48 h Postinjection

|         | blood | muscle | spleen | kidney | lung | heart | liver | intestine | stomach | tumor |
|---------|-------|--------|--------|--------|------|-------|-------|-----------|---------|-------|
| mouse 1 | 1.47  | 0.18   | 2.04   | 1.09   | 0.99 | 0.79  | 3.46  | 3.60      | 1.30    | 2.40  |
| mouse 2 | 1.33  | 0.49   | 2.23   | 1.21   | 1.29 | 1.21  | 3.22  | 2.22      | 0.66    | 2.15  |
| mouse 3 | 0.57  | 0.37   | 2.05   | 0.99   | 1.00 | 0.98  | 3.26  | 2.47      | 1.02    | 2.10  |
| average | 1.12  | 0.35   | 2.11   | 1.10   | 1.09 | 0.99  | 3.31  | 2.47      | 1.02    | 2.22  |
| SD      | 0.48  | 0.16   | 0.11   | 0.11   | 0.17 | 0.21  | 0.13  | 1.03      | 0.33    | 0.16  |

potassium iodide in water 24 h prior to injecting the labeled photosensitizer.

The maximum intensity of PS **4** in the tumor was observed at 24 h as determined by region of interest (ROI) calculations (data not given). However, for imaging, 48 h postinjection produced the best contrast, as it cleared more rapidly from liver, spleen, and intestine as compared to the tumor.

For comparing the biodistribution of PS **4** at 24, 48, 72, and 96 h postinjection, 3 mice/group were used and injected with comparatively lower radioactive dose (50 $\mu$Ci). The results are summarized in Figure 9. As can be seen, **4** produced good accumulation and circulation in tumor and blood, respectively, at 24 h postinjection. However, prominent uptake in the liver, spleen, and intestine was also observed. Interestingly, at 48 h postinjection, a much better ratio between tumor to liver, spleen, intestine, and muscle was observed (Figure 9, Table 1). At both time intervals (24 and 48 h), the tumor-to-muscle ratio was very high (6:1). PS **4** remains in the tumor until day 4, with less intensity due to fact that there was not enough drug present in the blood for circulation.

**Adjustment of Imaging (PET imaging) and Treatment Parameters.** From the results summarized in Figure 6, it can be seen that PS **2** produced excellent photosensitizing efficacy at a dose of 1.5 $\mu$mol/kg on exposing the tumors with light at 24 h postinjection. However, compared to 24-h images, enhanced PET images (better contrast) were observed at 48 h postinjection. For establishing the parameters for a "see and treat" approach, on exposing the tumors with a laser light (135 J/cm$^2$, 75 mW$^{2/}$cm$^2$ for 30 min) at 48 h postinjection, a significant decrease in PDT response was observed. Therefore, we made slight experimental modifications in our imaging and treatment parameters. In our modified protocol, the mice (five mice/group) were first injected with $^{124}$I-labeled PS **4** (50 $\mu$Ci), and after 24 h, the corresponding nonlabeled PS **2** was injected with a therapeutic dose (1.5 $\mu$mol/kg). After 24 h (i.e. 48 h after injecting **4**), the mice were imaged and the

light treatment was performed. The treatment outcome was excellent and was similar to that shown in Figure 6.

## Conclusions

To study compounds that have biological half-life times of days, radioisotopes with a physical half-life at similar length are required. $^{124}$I, with a half-life of 4.2 days, has an advantage over other nuclides with shorter-lived tracer-isotopes such as $^{18}$F (90 min) and $^{99m}$Tc (6 h). In this study we report the first synthesis of an $^{124}$I-labeled PS with high ($>$95%) radioactive specificity. The half-life time of the nuclide was found to be long enough to carry out the chemistry of the labeled PS and allow its accumulation in the target tissue while the drug clears from the nontarget organs. This is the first example that demonstrates that relatively selective accumulation of the porphyrin-based PS provides an opportunity for it to be utilized as a single agent for imaging (PET and optical) and therapy. The techniques employed in this study are noninvasive and the use of a single agent rules out any variability in the pharmacokinetics and pharmacodynamics pattern of the drug at any stage. This is in contrast to other studies, where either more than one agent or a bioconjugate molecule tethered with imaging probes is used, which could make significant changes in the pharmacokinetic and pharmacodynamic characteristics of the individual moieties. Our future investigations are focused on the synthesis of more tumor-avid iodo-photosensitizers (with and without $^{124}$I) exhibiting longer wavelength absorptions near the red region of the spectrum (near 800 nm), including a large Stokes shifts between the absorption and emission bands. These additional features will help to image and treat the large and deeply seated tumors by fluorescence imaging and PDT. A PS with PET and optical imaging also provides a unique opportunity to compare both the imaging modalities in a "see and treat" approach. Due to the high accumulation of porphyrin-based compounds in liver, kidney, and spleen, these photosensitizers may have limited application in imag-

ing those tumors that are located in these organs. However, these candidates could be promising candidates for imaging and treating lung, esophagus, breast, skin, oral, head, and neck cancer patients. For assessing the potential of the iodo analogue of pyropheophorbide-*a* and other photosensitizers, further studies with this and more tumor-avid photosensitizers in an orthotopic model are currently in progress. To improve tumor-specificity, efforts are also underway to develop photosensitizers for targeting those proteins that are known for their overexpression in tumor cells.

## Experimental Section

**Chemical Synthesis and Radioactive Labeling.** All chemicals were of reagent grade and used as such. Solvents were dried using standard methods. Reactions were carried out under nitrogen atmosphere and were monitored by precoated (0.20 mm) silica TLC plastic sheet (20 × 20 cm) strips (POLYGRAM SIL N-HR) and/or UV−visible spectroscopy. Silica gel 60 (70−230 mesh, Merck) was used for column chromatography. Melting points were determined on Fisher-Johns melting point apparatus and are uncorrected. UV−visible spectra were recorded on a Varian (Cary-50 Bio) spectrophotometer. $^1$H NMR spectra were recorded on Brucker AMX 400-MHz NMR spectrometer at 303 K in CDCl$_3$. Proton chemical shifts ($\delta$) are reported in parts per million (ppm) relative to CDCl$_3$ (7.26 ppm) or TMS (0.00 ppm). Coupling constants ($J$) are reported in Hertz (Hz) and s, d, t, q, p, m, and br refer to singlet, doublet, triplet, quartet, pentet, multiplet, and broad, respectively. Mass spectral data (electrospray ionization, ESI, by infusion) were obtained from Biopolymer Facility of Basic Studies Center, Roswell Park Cancer Institute. High-performance liquid chromatography was carried out on a system comprised of a Chrom Tech Iso-2000 pump, Hitachi L-4000 UV detector and a radiation detector. These detectors are connected to a computer with HP Chemstation software via HP 35900E interface. Bioscan system 200 imaging scanner was used for thin-layer chromatography of the radiolabeled compounds.

**Synthesis of Methyl 3-Devinyl-3-{1′-(*m*-iodobenzyloxy)-ethyl}pyropheophorbide-*a* (2).** Methyl pyropheophorbide-*a* (**1**) was obtained from chlorophyll-*a* by following the literature procedure.[34] **1** (100 mg) was reacted with 30% hydrobromic acid (HBr) in acetic acid (2 mL), and the reaction was stirred at room temperature for 2 h. After evaporating acids under high vacuum (0.1 mmHg), the residue was reacted with the *m*-iodobenzyl alcohol (excess). Dry dichloromethane (10 mL) and anhydrous potassium carbonate (40 mg) were added. The reaction mixture was stirred under nitrogen atmosphere for 45 min. It was then diluted with dichloromethane (200 mL) and washed with aqueous sodium bicarbonate solution (1 × 100 mL) and then with water (2 × 200 mL). The dichloromethane layer was separated and treated with diazomethane and dried over anhydrous sodium sulfate. Evaporation of the solvent gave a syrupy residue, which was chromatographed over silica column using hexanes:ethyl acetate 4:1 as eluant to remove excess *m*-iodobenzyl alcohol followed by hexanes:ethyl acetate 1:1 to yield the desired compound **2**. Yield: 115 mg (80%). Mp: 112−114 °C. UV−vis (CH$_2$Cl$_2$): 662 (4.75 × 10$^4$), 536 (1.08 × 10$^4$), 505 (1.18 × 10$^4$), 410 (1.45 × 10$^5$). $^1$H NMR (CDCl$_3$; 400 MHz): $\delta$ 9.76, 9.55 and 8.56 (all s, 1H, meso-H), 7.76 (s, 1H, ArH), 7.64 (d, $J$ = 6.8, 1H, ArH), 7.30 (d, $J$ = 8.0, 1H, ArH), 7.05 (t, $J$ = 8.2, 1H, ArH), 6.00 (q, $J$ = 6.9, 1H, 3$^1$-H), 5.28 (d, $J$ = 19.8, 1H, 13$^2$-CH$_2$), 5.13 (d, $J$ = 19.8, 1H, 13$^2$-CH$_2$), 4.70 (d, $J$ = 12.0, 1H, OCH$_2$Ar), 4.56 (dd, $J$ = 3.2,11.6, 1H, OCH$_2$Ar), 4.48−4.53 (m, 1H, 18-H), 4.30−4.33 (m, 1H, 17-H), 3.72 (q, $J$ = 8.0, 2H, 8-C*H*$_2$CH$_3$), 3.69, 3.61, 3.38 and 3.21 (all s, all 3H, for 17$^3$-CO$_2$CH$_3$ and 3 × ring CH$_3$), 2.66−2.74, 2.52−2.61, and 2.23−2.37 (m, 4H, 17$^1$ and 17$^2$-H), 2.18 (dd, $J$ = 2.8, 6.4, 3H, 3$^2$-CH$_3$), 1.83 (d, $J$ = 8.0, 3H, 18-CH$_3$), 1.72 (t, $J$ = 7.6, 3H, 8-CH$_2$C*H*$_3$), 0.41 (brs, 1H, NH), −1.71 (brs, 1H, NH). HRMS

for C$_{41}$H$_{43}$N$_4$O$_4$I: 782.2329 (calcd), 783.2407 (found, MH$^+$). Anal. Calcd For C$_{41}$H$_{43}$N$_4$O$_4$I: C, 62.91; H, 5.54; N, 7.16; I, 16.21. Found: C, 62.60; H, 5.59; N, 7.13; I, 16.45.

**Synthesis of Methyl 3-Devinyl-3-{1′-(*m*-trimethylstannylbenzyloxy)ethyl}pyropheophorbide-*a* (3).** To a solution of methyl 3-devinyl-3-{1-(*m*-iodobenzyloxy)ethyl}pyropheophorbide-*a* (**2**) (10 mg) in degassed 1,4-dioxane(5 mL) were added hexamethyldistannane (0.1 mL) and bis(triphenylphosphine)palladium(II) dichloride (2 mg), and the reaction mixture was stirred at 60 °C for overnight time.[5] After rotavapoing to dryness, the crude mixture was purified by prep-HPLC using a Phenomenex Luna 10 $\mu$m silica 100 A 250 × 10 mm column. Hexane:ethyl acetate (70:30) was used as eluant to yield compound **3**. Yield: 9 mg (85%). $^1$H NMR (CDCl$_3$; 400 MHz): $\delta$ 9.76, 9.54 and 8.55 (all s, 1H, meso-H), 7.43 (m, 2H, ArH), 7.36 (m, 2H, ArH), 6.01 (q, $J$ = 6.7, 1H, 3$^1$-H), 5.27 (d, $J$ = 19.1, 1H, 13$^2$-CH$_2$), 5.12 (d, $J$ = 19.1, 1H, 13$^2$-CH$_2$), 4.78 (dd, $J$ = 5.4, 11.9, 1H, OCH$_2$Ar), 4.61 (dd, $J$ = 1.7,12.0, 1H, OCH$_2$-Ar), 4.50 (q, $J$ = 7.4, 1H, 18-H), 4.32 (d, $J$ = 8.8, 1H, 17-H), 3.72 (q, $J$ = 7.8, 2H, 8-C*H*$_2$CH$_3$), 3.69, 3.61, 3.37 and 3.18 (all s, all 3H, for 17$^3$-CO$_2$CH$_3$ and 3 × ring CH$_3$), 2.66−2.75, 2.52−2.61, and 2.23−2.37 (m, 4H, 17$^1$ and 17$^2$-H), 2.16 (m, 3H, 3$^2$-CH$_3$), 1.83 (d, $J$ = 7.2, 3H, 18-CH$_3$), 1.72 (t, $J$ = 7.6, 3H, 8-CH$_2$C*H*$_3$), 0.45 (brs, 1H, NH), 0.19 (s, 9H, *tert*-butyltin), −0.59 (brs, 1H, NH). Mass calcd for C$_{45}$H$_{52}$N$_4$O$_4$Sn 831, found: 854 (M$^+$ + Na). Anal. Calcd for C$_{45}$H$_{52}$N$_4$O$_4$Sn: C, 64.99; H, 6.30; N, 6.74. Found: C, 64.56; H, 6.66; N, 6.59.

**Synthesis of Methyl [$^{124}$I]-3-Devinyl-3-{1′-(*m*-iodobenzyloxy)ethyl}pyropheophorbide-*a* (4).** The trimethyltin analogue **3** (50 $\mu$g) was dissolved in 50 $\mu$L of 10% acetic acid in methanol, and 100 $\mu$L of 10% acetic acid in methanol was added to Na$^{124}$I in 10 $\mu$L of 0.1 N NaOH. The two solutions were mixed and an IODOGEN bead was added.[33] The reaction mixture was incubated at room temperature for 30 min and the reaction product was injected on a HPLC column (Phenomenex Maxsil C8 5 $\mu$m), which was eluted with a 90:10 mixture of methanol and water at a flow rate of 1 mL/min. The labeled product was collected.

**In Vitro Uptake.** The RIF tumor cells were utilized for determining drug uptake. RIF cells were grown in $\alpha$-MEM with l-glutamine, penicillin, streptomycin, and neomycin. Cells were maintained in complete media at 5% CO$_2$, 95% air, and 100% humidity. Approximately 1.5 × 10$^5$ cells per well were seeded in 6-well plates. After an overnight incubation at 37 °C, the media was aspirated and fresh media (3 mL/well) was added. The photosensitizers at 0.25 $\mu$M were added (three wells/photosensitizer) and incubated in the dark at 37 °C for 3 and 24 h. Drug-containing media was removed; cells were washed with PBS (without Ca$^{2+}$), and 1 mL of Solvable (PerkinElmer Life and Analytical Sciences) was added to each well to solubilize the cells. The plates were incubated in the dark at 37 °C for 2 h. After the incubation time, 2 mL of doubly distilled H$_2$O was added to each well and the fluorescence was read (ex 415 nm, em 667 nm) on a FluoroMax-2 instrument (ISA, JOBIN YVON-SPEX, Horiba Group). The protein content of the 3-mL sample was determined using the Bio-Rad DC assay. The data were plotted as fluorescence/(mg/mL of protein).

**Subcellular Localization.** RIF cells were grown on poly-L-lysine-coated coverslips in 6-well plates and incubated in growth medium for different times with compound **2**. Fluorescent compounds (Molecular Probes) specific for different subcellular organelles were co-incubated with compound **2** prior to examination by fluorescence microscopy [for mitochondria, Mitotracker Green (MTG), 1 $\mu$M for 1 h prior to examination; for lysosomes, Fluospheres 505/515 yellow green 0.1 $\mu$m diameter 1/10 000 dilution for 24 h with gentle rocking; for the Golgi apparatus, Bodipy FL C5 Ceramide in the form of bovine serum albumin (BSA) complexes, 5 $\mu$M as directed by manufacturer's protocol]. Cells were examined using a Zeiss Axiovert 200 inverted microscope, with a Fluoarc mercury vapor short-arc lamp as light source. Images were collected with the AxioCam MR-MRGrab frame grabber and processed with AxioVision LE 4.1 imaging software. The individual

fluorochromes were examined with the following filter combinations from ChromaTechnology: for compound **2**, Ex BP D410/40, BeamSplitter FT 505dcxvu, Em BP 675/50; for MTG and Fluospheres, Set 38 1031-346, Ex BP 470/40, BeamSplitter FT 495, Em BP 525/50; for Bodipy C5 Ceramide, Set 31 1031-350, Ex BP 565/30, BeamSplitter FT 585, Em BP 520/60.

**Competitive Peripheral Benzodiazepine Receptor Binding.** To labeled, 5-mL disposable glass borosilicate tubes were added $1 \times 10^6$ RIF cells in 50 $\mu$L of Tris buffer (25 mM, pH 7.4), 50 $\mu$L of $^3$H-PK11195 (45 nM final concentration), and 50 $\mu$L of competitor (cold PK11195 or photosensitizers). Final concentrations (molar) of the competitors were $1 \times 10^9$, $1 \times 10^{-8}$, $1 \times 10^{-7}$, $5 \times 10^{-7}$, $1 \times 10^{-6}$, $5 \times 10^{-6}$, $1 \times 10^{-5}$, $5 \times 10^{-5}$, $1 \times 10^{-4}$ diluted in Tris buffer. The background control contained no cells, 50 $\mu$L of $^3$H-PK11195, and 100 $\mu$L of Tris buffer, and the maximum binding control contained 50 $\mu$L of Tris buffer instead of competitor. Samples were incubated for 1 h at 4 °C and then the incubation was inhibited by dilution with 3 mL of Tris buffer. The cells were filtered by vacuum on GF/C Whatman filters presoaked in Tris buffer containing 0.5% polyethyleneimine [(Sigma) to prevent nonspecific binding to the filter] and the filters were washed 3 times each with 4 mL of Tris buffer. The filters were transferred to scintillation vials, and 4 mL of scintillation fluid (Universol, ICN) was added. The vials were shaken to dissolve $^3$H-PK11195 and left in the dark to equilibrate, and the radioactivity of the samples was counted in a $\beta$-counter. The concentration of competitor at which 50% of $^3$H-PK11195 binding was inhibited (IC$_{50}$) was calculated to determine the binding of competitors compared relative to PK11195.

**In Vitro Photosensitizing Efficacy.** The photosensitizing activity of **2** was determined in the RIF tumor cell line. The RIF tumor cells were grown in α-MEM with 10% fetal calf serum, l-glutamine, penicillin, streptomycin, and neomycin. Cells were maintained in 5% CO$_2$, 95% air, and 100% humidity. For determining the PDT efficacy, these cells were plated in 96-well plates at a density of $5 \times 10^3$ cells/well in complete media. After an overnight incubation at 37 °C, the photosensitizers were added at variable concentrations and incubated at 37 °C for 24 h in the dark. Prior to light treatment, the cells were replaced with drug-free complete media. Cells were then illuminated with an argon-pumped dye laser set at 665 nm at a dose rate of 3.2 mW/cm$^2$ for 0–4 J/cm$^2$. After PDT, the cells were incubated for 48 h at 37 °C in the dark. Following the 48-h incubation, 10 $\mu$L of 5.0 mg/mL solution of 3-[4,5-dimethylthiazol-2-yl]-2,5-diphenyltetrazoliumbromide (MTT) dissolved in PBS (Sigma, St. Louis, MO) was added to each well. After a 4-h incubation at 37 °C, the MTT and media were removed, and 100 $\mu$L of DMSO was added to solubilize the formazin crystals. The 96-well plate was read on a microtiter plate reader (Miles Inc., Titertek Multiscan Plus MK II) at an absorbance of 560 nm. The results were plotted as percent survival of the corresponding dark (drug no light) control for each compound tested. Each data point represents the mean from three separate experiments, and the error bars are the standard deviation. Each experiment was done with five replicate wells.

**In Vivo Photosensitizing Efficacy.** The C3H mice were subcutaneously injected with $3 \times 10^5$ RIF cells in 30 $\mu$L complete α-MEM (into the axilla), and tumors were grown until they reached 4–5 mm in diameter. The day before laser light treatment, all hair was removed from the inoculation site and the mice were injected intravenously with varying photosensitizer concentrations. At 24 h postinjection, the mice were restrained without anesthesia in plastic holders and then treated with laser light from an argon-pumped dye laser tuned to emit drug-activating wavelengths as set by the monochromator (665 nm). The treatment parameters desired consisted of a diameter size of 1 cm$^2$ and a fluence rate of 75 mW/cm$^2$ for a total light dose of 135 J/cm$^2$. The mice were observed daily for signs of weight loss, necrotic scabbing, or tumor regrowth. If tumor growth appeared, the tumors were measured using two orthogonal measurements $L$ and $W$ (perpendicular to $L$), and the volumes were calculated using the formula $V = (LW^2)/2$ and recorded. Mice were considered cured if there was no sign of tumor regrowth by day 60 after PDT treatment.

**PET Imaging.** Mice were imaged in the micropet FOCUS 120, a dedicated 3D small-animal PET scanner (Concorde Microsystems Inc.) at State University of New York at Buffalo (South Campus) under the Institutional Animal Care and Use Committee (IACUC) guidelines. All control ($n = 4$) and tumored ($n = 4$) C$_3$H mice were injected via the tail vein with 36–104 $\mu$Ci of **4**, and after 24, 48, 72, and 96h postinjection, the mice were anesthetized by inhalation of isoflurane/oxygen, placed head first, prone for imaging, and the acquisition time was set for 30 min. No efforts were made to block the radioiodine uptake by thyroid or stomach, and surprisingly, in only a few cases was a little bit of radioiodine uptake observed in the thyroid, and that too was cleared by 72 h. Some control and tumored mice were also imaged using F-18-FDG radiotracer 24 h prior to $^{124}$I imaging. These mice were administered 150–200 $\mu$Ci of F-18-FDG via the tail vein and were scanned for 20 min in the fashion described above, beginning 45 min after FDG injection.

**Fluorescence Imaging.** In vivo fluorescence imaging was accomplished by using a Illumination Dual Light System (Lightools Research, Encinitas, CA), designed for small animal studies. True-Color fluorescence images were obtained using dielectric long-pass filters (Chroma Tech) and a digital color camera (Optronics, Magnafire SP, Olympus America). Wavelength-resolved spectral imaging was carried out by using a Nuance multispectral imaging system (CRI, Inc., Woburn, MA) comprising an optical head that includes Varispec liquid crystal tunable filters (LCTFs, with a bandwidth of 20 nm and a scanning wavelength range of 400–720 nm), an optical coupler, and a high-resolution scientific-grade CCD camera, along with image acquisition and analysis software. The tunable filter was automatically stepped in 10-nm increments from 550 to 720 nm while the camera captured images at each wavelength with a constant exposure. The 18 resulting TIFF images were loaded into a single data structure in memory, forming a spectral stack with a spectrum at every pixel. Autofluorescence spectra and PS fluorescence spectra were manually selected from the spectral image using the computer mouse to select appropriate regions. Spectral unmixing algorithms (available from CRI, Inc.) were applied to create the unmixed images of pure autofluorescence and pure PS fluorescence signal, as shown in Figure 7.

Using an IACUC-approved protocol, the C3H mice were subcutaneously injected with $3 \times 10^5$ RIF cells in 30 $\mu$L of complete α-MEM (into the right posterior axilla), and tumors were grown until they reached 4–5 mm in diameter. The day before PS injection, all hairs were removed from the inoculation site and the mice were imaged under anesthesia (IP injection of ketamine and xylazine mixture). In a dark box, illumination was provided by fiber optic lighting at 540/40x nm (green color), and a long-pass filter was used to reject scattering and to pass Stoke-shifted PS fluorescence at 667 nm. Under similar conditions, mice were imaged at 24, 48, and 72 h postinjection of the PS (1.5 $\mu$mol/kg). After whole-body imaging, the tumor was surgically removed from the original site (axilla) and placed on a shaved region of skin away from the original site as a means to image the skin flap (minus the tumor).

**Biodistribution Studies. $\gamma$-Well Counter.** All studies were performed as per IACUC guidelines. The mice were injected with 15–50 $\mu$Ci of **4** via tail vein, and three mice each at 24, 48, 72, and 96 h time interval were sacrificed, and body organs (tumor, heart, liver, spleen, kidney, lung, muscle, etc.) were removed immediately. After weighing, the amount of radioactivity in the tumor (300–400 mg), body organs, and blood was measured by a $\gamma$-well counter. Radioactivity uptake was calculated as the percentage of the injected dose per gram of the tissue (%ID/g). Statistical analyses and data (%ID/g vs time point) were plotted using Microsoft Excel.

## References

(1) Massoud, T. F.; Gambhir, S. S. Molecular imaging in living subjects: Seeing fundamental biological processes in a new light. *Genes Dev.* **2003**, *17*, 545−580.

(2) Rudin, M.; Weissleder, R. Molecular imaging in drug discovery and development. *Nature Rev. Drug Discovery* **2003**, *2*, 123−131.

(3) Phelps, M. E. Inaugural article: Positron emission tomography provides molecular imaging of biological processes. *Proc. Natl. Acad. Sci. U.S.A.* **2000**, *97*, 9226−9233.

(4) Verel, I.; Vissser, G. W. M.; van Dongen, G. A. M. S. The promise of immuno-PET in radioimmunotherapy. *J. Nucl. Med.* **2005**, *46*, 164S-171S.

(5) Koziorowski, J.; Henssen, C.; Weinreich, R A new convenient route to radioiodinated N-succinimidyl 3- and 4-iodobenzoate, two reagents for radioiodination of proteins. *Appl. Radiat. Isot.* **1998**, *49*, 955−959.

(6) Verel, I.; Visser, G. W. M.; Vosjan, M. J. W. D.; Finn, R.; Boellaard, R.; van Dongen, G. A. M. S. High-quality 124I-labeled monoclonal antibodies for use as PET scouting agents prior to 131I-radioimmunotherapy. *Eur. J. Nucl. Med. Mol. Imaging* **2004**, *31*, 1645−1652.

(7) Pentlow, K. S.; Graham, M. C.; Lambrecht, R. M.; Cheung, N.-K. V.; Larson, S. M. Quantitative imaging of I-124 using positron emission tomography with applications to radioimmunodiagnosis and radioimmunotherapy. *Med. Phys.* **1991**, *18*, 357−366.

(8) Wilson, C. B.; Snook, D. E.; Dhokia, B.; Taylor, C. V.; Watson, I. A.; Lammertsma, A. A.; Lambrecht, R.; Waxman, J.; Jones, T.; Epenetos, A. A. Quantitative measurement of monoclonal antibody distribution and blood flow using positron emission tomography and 124iodine in patients with breast cancer. *Int. J. Cancer* **1991**, *47*, 344−347.

(9) Petlow, K. S.; Graham, M. C.; Lambrecht, R. M.; Daghighian, F.; Bacharach, S. L.; Bendriem, B.; Finn, R. D.; Jordan, K.; Kalaigian, H.; Karp, J. S.; Robeson, W. R.; Larson, S. M. Quantitative imaging of iodine-124 with PET. *J. Nucl. Med.* **1996**, *37*, 1557−1562.

(10) Gonzalez Trotter, D. E.; Manjeshwar, R. M.; Doss, M.; Shaller, C.; Robinson, M. K.; Tandon, R.; Adams, G. P.; Adler, L. P. Quantitation of small-animal (124)I activity distributions using a clinical PET/CT scanner. *J. Nucl. Med.* **2004**, *45*, 1237−1244.

(11) Sgouros, G.; Kolbert, K. S.; Sheikh, A.; Pentlow, K. S.; Mun, E. F.; Barth, A.; Robbins, R. J.; Larson, S. M. Patient-specific dosimetry for 131I thyroid cancer therapy using 124I PET and 3-dimensional-internal dosimetry (3D-ID) software. *J. Nucl. Med.* **2004**, *45*, 1366−1372.

(12) Lee, F. T.; Hall, C.; Rigopoulos, A.; Zewit, J.; Pathmaraj, K.; O′Keefe, G. J.; Smyth, F. E.; Welt, S.; Old, L. J.; Scott, A. M. Immuno-PET of human colon xenograft- bearing Balb/c nude mice using 124I−CDR-grafted humanized A33 monoclonal antibody. *J. Nucl. Med.* **2001**, *42*, 764−769.

(13) Sundaresan, G.; Yazaki, P. J.; Shively, J. E.; Finn, R. D.; Larson, S. M.; Raubitschek, A. A.; Williams, L. E.; Chatziioannou, A. F.; Gambhir, S. S.; Wu, A. M. 124I-labeled engineered anti-CEA minibodies and diabodies allow high-contrast, antigen-specific small-animal PET imaging of xenografts in athymic mice. *J. Nucl. Med.* **2003**, *44*, 1962−1969 and related references therein.

(14) Collingride, D. R.; Glaser, M.; Osman, S.; Barthel, H.; Hutchinson, O. C.; Luthra, S. K.; Brady, F.; Hayes, L. B.; Martin, S. J.; Workman, P.; Price, P.; Aboagye, E. O. In vitro selectivity, in vivo biodistribution and tumour uptake of annexin V radiolabelled with a positron emitting radioisotope. *Br. J. Cancer* **2003**, *89*, 1327−1333.

(15) Zanzonico, P.; O'Donoghue, J.; Chapman, J. D.; Schneider, R.; Cai, S.; Larson, S.; Wen, B.; Chen, Y.; Finn, R.; Ruan, S.; Gerweck, L.; Humm, J.; Ling, C. Iodine-124-labeled iodo-azomycin-galactoside imaging of tumor hypoxia in mice with serial microPET scanning. *Eur. J. Nucl. Med. Mol. Imaging* **2004**, *31*, 117−128.

(16) Bennett, J. J.; Tjuvajev, J.; Johnson, P.; Doubrovin, M.; Akhurst, T.; Malholtra, S.; Hackman, T.; Balatoni, J.; Finn, R.; Larson, S. M.; Federoff, H.; Blasberg, R.; Fong, Y. Positron emission tomography imaging for herpes virus infection: Implications for oncolytic viral treatments of cancer. *Nature Med.* **2001**, *7*, 859−863.

(17) Doubrovin, M.; Ponomarev, V.; Beresten, T.; Balatoni, J.; Bornmann, W.; Finn, R.; Humm, J.; Larson, S.; Sadelain, M.; Blasberg, R.; Tjuvajev, J. G. Imaging transcriptional regulation of p53-dependent genes with positron emission tomography in vivo. *Proc. Natl. Acad. Sci. U.S.A.* **2001**, *98*, 9300−9305.

(18) Jacobs, A.; Voges, J.; Reszka, R.; Lercher, M.; Gossmann, A.; Kracht, L.; Kaestle, Ch.; Wagner, R.; Weinhard, K.; Heiss, W. D. Positron-emission tomography of vector-mediated gene expression in gene therapy for gliomas. *Lancet* **2001**, *358*, 727−729.

(19) Koehne, G.; Doubrovin, M.; Doubrovina, E.; Zanzonico, P.; Gallardo, H. F.; Ivanova, A.; Balatoni, J.; Feldstein, J. T.; Heller, G.; May, C.; Ponomarev, V.; Ruan, S.; Finn, R.; Blasberg, R. G.; Bornmann, W.; Riviere, I.; Sadelain, M.; O'Reilly, R. J.; Larson, S. M.; Tjuvajev, J. G. Serial *in vivo* imaging of the targeted migration of human HSV-TK-transduced antigen-specific lymphocytes. *Nature Biotechnol.* **2003**, *21*, 405−413.

(20) Soghomonyan, S. A.; Doubrovin, M.; Pike, J.; Luo, X.; Ittensohn, M.; Runyan, J. D.; Balatoni, J.; Finn, R.; Tjuvajev, J. G.; Blasberg, R.; Bermudes, D. Positron emission tomography (PET) imaging of tumor-localized Salmonella expressing HSV1-TK. *Cancer Gene Ther.* **2005**, *12*, 101−108.

(21) Moore, J. V.; Waller, M. L.; Zhao, S.; Dodd, N. J. F.; Acton, P. D.; Jeavons, A. P.; Hastings, D. L. Feasibility of imaging photodynamic injury to tumours by high-resolution positron emission tomography. *Eur. J. Nucl. Med.* **1998**, *25*, 1248−1254.

(22) Dong, D.; Dubeau, L.; Bading, J.; Nguyen, K.; Luna, M.; Yu, H.; Bornstein, G. G.; Gordon, E. M.; Gomer, C.; Hall, F. L.; Gambhir, S. S.; Lee, A. S. Spontaneous and controllable activation of suicide gene expression driven by the stress-inducible grp78 promoter resulting in eradication of sizable human tumors. *Human Gene Ther.* **2004**, *15*, 553−561.

(23) Sugiyama, M.; Sakahara, H.; Sato, K.; Harada, N.; Fukumoto, D.; Kakiuchi, T.; Hirano, T.; Kohno, E.; Tsukada, H. Evaluation of 3′-deoxy-3′-18F-fluorothymidine for monitoring tumor response to radiotherapy and photodynamic therapy in mice. *J. Nucl. Med.* **2004**, *45*, 1754−1758.

(24) Westermann, P.; Glanzmann, T.; Andrejevic, S.; Braichotte, D. R.; Forrer, M.; Wagnieres, G. A.; Monnier, P.; Van den Bergh, H.; Mach, J.-P.; Folli, S. Long circulating half-life and high tumor selectivity of the photosensitizer meta-tetrahydroxyphenylchlorin conjugated to polyethylene glycol in nude mice grafted with a human colon carcinoma. *Int. J. Cancer* **1998**, *76*, 842−850.

(25) Ma, B.; Li, G.; Kanter, P.; Lamonica, D.; Grossman, Z.; Pandey, R. K. Bifunctional HPPH−N2S2 TC-99m conjugates as tumor imaging agents: Synthesis and biodistribution studies. *J. Porphyrins Phthalocyanines* **2003**, *1*, 500−507.

(26) Chen, Y.; Zheng, X.; Dobhal, M. P.; Gryshuk, A.; Morgan, J.; Dougherty, T. J.; Oseroff, A.; Pandey, R. K. Methyl pyropheophorbide-a analogues: Potential fluorescent probes for the peripheral-type benzodiazepine receptors. Effect of central metal in photosensiting efiicacy. *J. Med. Chem.* Accepted.

(27) Ntziachristos, V.; Ripoll, J.; Wang, L. V.; Weissleder R. Looking and listening to light: The evolution of whole-body photonic imaging. *Nature Biotechnol.* **2005**, *23*, 313−20.

(28) Ghoroghchian, P. P.; Frail, P. R.; Susumu, K.; Blessington, D.; Brannan, A. K.; Bates, F. S.; Chance, B.; Hammer, D. A.; Therien, M. J. Near-infrared-emissive polymersomes: Self-assembled soft matter for in vivo optical imaging. *Proc. Natl. Acad. Sci. U.S.A.* **2005**, *102*, 2922−2927.

(29) Achilefu, S.; Jimenez, H. N.; Dorshow, R. B.; Bugaj, J. E.; Webb, E. G.; Wilhelm, R. R.; Rajagopalan, R.; Johler, J.; Erion, J. L. Synthesis, in vitro receptor binding, and in vivo evaluation of fluorescein and carbocyanine peptide-based optical contrast agents. *J. Med. Chem.* **2002**, *45*, 2003−2015.

(30) Ye, Y.; Bloch, S.; Kao, J.; Achilefu, S. Multivalent carbocyanine molecular probes: Synthesis and applications. *Bioconjugate Chem.* **2005**, *16*, 51−61.

(31) Henderson, B. W.; Bellnier, D. A.; Greco, W. R.; Sharma, A.; Pandey, R. K.; Vaughan, L.; Weishaupt, K. R.; Dougherty, T. J. An in vivo quantitative structure−activity relationship for a congeneric series of pyropheophorbide derivatives as photosensitizers for photodynamic therapy. *Cancer Res.* **1997**, *57*, 4000−4007.

(32) Zhang, M.; Zhang, Z.; Blessington, D.; Li, H.; Busch, T. M.; Madrak, V.; Miles, J.; Chance, B.; Glickson, J. D.; Zheng, G. Pyropheophorbide 2-deoxyglucosamide: New photosensitizer targeting glucose transporters. *Bioconjugate Chem.* **2003**, *14*, 709−714.

(33) Gurfinkel, M.; Thompson, A. B.; Ralston, W.; Troy, T. L.; Moore, A. L.; Moore, T. A.; Gust, J. D.; Tatman. D.; Reynolds, J. S.; Muggenburg, B.; Nikula, K.; Pandey, R.; Mayer, R. H.; Hawrysz, D. J.; Sevick-Muraca, E. M. Pharmacokinetics of ICG and HPPH-car for the detection of normal and tumor tissue using fluorescence, near-infrared reflectance imaging: A case study. *Photochem. Photobiol.* **2000**, *74*, 94−102.

(34) Pandey, R. K.; Sumlin, A. B.; Constantine, S.; Aoudia, M.; Potter, W. R.; Bellnier, D. A.; Henderson, B. W.; Rodgers, M. A.; Smith, K. M.; Dougherty, T. J. Alkyl ether analogues of chlorophyll-a derivatives: Part 1. Synthesis, photophysical properties and photodynamic efficacy. *Photochem. Photobiol.* **1996**, *64*, 194–204.

(35) Kozikowski, A. P.; Kotoula, M.; Ma, D.; Boujrad, N.; Tuckmantel, W.; Papadopoulos, V. Synthesis and biology of a 7-nitro-2,1,3-benzoxadiazol-4-yl derivative of 2-phenylindole-3-acetamide: A fluorescent probe for the peripheral-type benzodiazepine receptor. *J. Med. Chem*, **1997**, *40* (16), 2435–2439 and the references therein.

(36) Han, Z.; Slack, R. S.; Li, W. P.; Papadopoulos, V. Expression of peripheral benzodiazepine receptor (PBR) in human tumors: Relationship to breast, colorectal, and prostate tumor progression. *J. Recept. Signal Transduct.* **2003**, *23*, 225–238.

(37) Dougherty, T. J.; Sumlin, A. B.; Greco, W. R.; Weishaupt, K. R.; Vaughan, L. A.; Pandey, R. K. The role of the peripheral benzodiazepine receptor in photodynamic activity of certain pyropheophorbide ether photosensitizers: Albumin site II as a surrogate marker for activity. *Photochem. Photobiol.* **2002**, *76* (1), 91–97.

(38) Busch, T. M.; Wileyto, E. P.; Emanuele, M. J.; Piero, F. D.; Marconato L.; Glastein E. and Koch, C. J. Photodynamic therapy creates fluence rate-dependent gradients in the intratumoral spatial distribution of oxygen. *Cancer Res.* **2002**, *62*, 7273–7279.

(39) Wilson, B. C.; Patterson, M. S. and Lilge, L. Implicit and explicit dosimetry in photodynamic therapy: A new paradigm. *Lasers Med. Sci.* **1997**, *12*, 182–199.